1

Design of Low-Cost Probe-Fed Microstrip Antennas

D. C. Nascimento and J. C. da S. Lacava
Technological Institute of Aeronautics
Brazil

1. Introduction

The concept of microstrip radiators, introduced by Deschamps in 1953, remained dormant until the 1970s when low-profile antennas were required for an emerging generation of missiles (James & Hall, 1989; Garg et al., 2001; Volakis, 2007). Since then, but mainly over the last three decades, the international antenna community has devoted much effort to theoretical and experimental research on this kind of radiator (Lee & Chen, 1997). Currently, low-loss RF laminates are used in their fabrication and many of their inherent limitations have been overcome (Garg et al., 2001). On the other hand, low-cost solutions are in demand now that both market and technology are ready for mass production (Gardelli et al., 2004). Recently, the design of single-fed circularly-polarized (CP) microstrip antennas manufactured with FR4 substrate was reported (Niroojazi & Azarmanesh, 2004). Unfortunately, the use of low-cost FR4 as the substrate introduces some additional complexity on the antenna design. This is due to the inaccuracy of the FR4 relative permittivity and its high loss tangent (around 0.02). Variations in the FR4 electrical permittivity can shift the operating frequency and the high loss tangent dramatically affects the antenna axial ratio and gain, resulting in poor radiation efficiency. To increase the efficiency, microstrip antenna on moderately thick substrate must be designed. However, the technique used to compensate for the probe inductance, when the patch is fed by a coaxial probe (a known practical way to feed microstrip antennas), still relies on the designer's expertise. For instance, a series capacitor, which may be constructed in several ways, has been utilized to neutralize this inductance (Hall, 1987; Alexander, 1989; Dahele et al., 1989; Vandenbosch & Van de Capelle, 1994; Nascimento et al., 2006), or the probe geometry has been modified (Haskins & Dahele, 1998; Teng et al., 2001; Chang & Wong, 2001; Tzeng et al., 2005). Unfortunately, due to their complexity, many such techniques are not suitable when the antennas are series-produced in an assembly line.

To overcome some of the abovementioned issues, two efficient techniques for designing low-cost probe-fed microstrip antennas are proposed. Using only their intrinsic characteristics, linearly- and circularly-polarized microstrip antennas can now be designed without the need for any external matching network. Limitations of the proposed approach will also be discussed. The chapter is organized as follows: Section 2 covers the design of linearly-polarized microstrip antennas; results obtained with the new approach are compared with those using the standard design technique. Circularly-polarized antennas

are addressed in Section 3 and experimental results are shown in Section 4. Other applications using the new design approach are presented in Section 5, and finally in Section 6, conclusions are drawn from the obtained results.

2. Linearly-polarized microstrip antennas

The typical geometry of a rectangular-patch linearly-polarized (LP) microstrip antenna is shown in Fig. 1, where a denotes the patch length, b the radiating edge width, p the probe position along the x-axis, and h the substrate thickness. The patch is printed on a finite rectangular substrate of dimensions (L by W) in order to avoid the excitation of surface waves, and the antenna is directly fed by a 50-Ω SMA connector. The analysis carried out in this section is focused on this particular radiator.

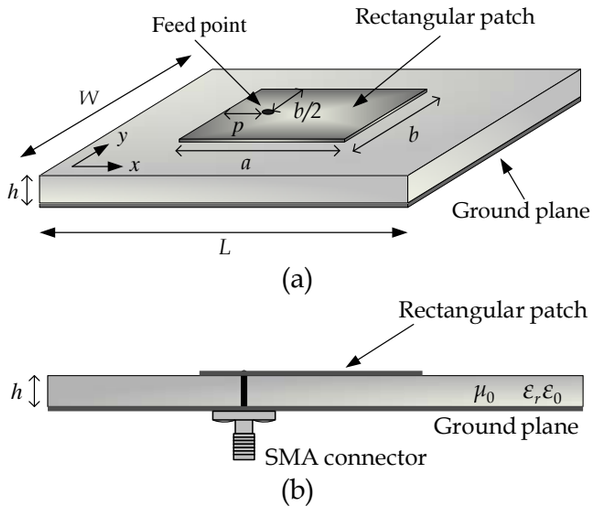

Fig. 1. Linearly-polarized probe-fed microstrip antenna: (a) top view – (b) side view.

2.1 Radiation efficiency

The radiation efficiency is defined as the ratio of the total power radiated (P_r) by an antenna to the net power accepted (P_{in}) by the antenna from the connected transmitter (IEEE Std 145, 1993). Since the antenna under consideration has its dielectric truncated, the cavity model, although originally developed for the analysis of electrically thin microstrip antennas, can be used for estimating the efficiency behavior. For the microstrip antenna shown in Fig. 1, the geometry of its equivalent cavity, neglecting the fringe effect, is given in Fig. 2. Under the condition $h << a < b$, the electric field of the TM_{mn} resonant mode excited within the cavity is expressed by

$$E_z = \frac{V_{mn}}{h}\cos\left(\frac{m\pi x}{a}\right)\cos\left(\frac{n\pi y}{b}\right), \tag{1}$$

where V_{mn}/h denotes the electric field intensity on the magnetic walls.
In case of linearly-polarized antenna excited in the fundamental TM_{10} mode, the dielectric (P_d) and metallic (P_m) losses can be calculated by means of equations (2) and (3), respectively.

$$P_d = \frac{\sigma_d}{2}\int_V |E_z|^2 dV = \frac{V_{10}^2\, ab\sigma_d}{4h}, \tag{2}$$

$$P_m = \frac{R_s}{2}\int_S |\vec{J}_s|^2 dS = \frac{V_{10}^2\, R_s\, ab\varepsilon_0\varepsilon_r}{2h^2\mu_0}, \tag{3}$$

where ε_r is the substrate relative permittivity, σ_d its electric conductivity, $\vec{J}_s$ the surface electric current density on the metallic walls, R_s the surface resistance, and ε_0 and μ_0 are the electric permittivity and magnetic permeability of free space, respectively.

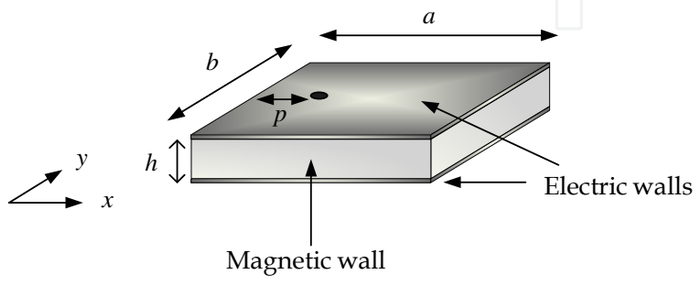

Fig. 2. Geometry of the antenna equivalent cavity.

The radiated power can be obtained by computing

$$P_r = \int_0^{2\pi}\int_0^{\pi/2} \frac{1}{2\eta_0}\left(|E_\theta|^2 + |E_\phi|^2\right) r^2 \operatorname{sen}\theta d\theta d\phi, \tag{4}$$

where η_0 denotes the free-space intrinsic impedance and E_θ and E_ϕ are the components of the far electric field radiated by the antenna, evaluated using Huygens's magnetic current source approach (Lumini et al., 1999).

Neglecting the surface wave losses, since the antenna has its dielectric truncated, the radiation efficiency can be estimated by the following expression

$$\eta = \frac{P_r}{P_d + P_m + P_r}. \tag{5}$$

Using equations (1) – (5), the radiation efficiency of LP antennas, designed to operate at 1.575 GHz in the fundamental TM_{10} mode, were calculated, and the results are shown in Fig. 3. In Fig. 3(a), the radiation efficiency curves of a 1.524-mm thick LP antenna are plotted as a function of the dielectric loss tangent, with the substrate relative permittivity as a parameter. In Fig. 3(b), graphics of radiation efficiency are presented, for the case of a rectangular patch printed on the FR4 laminate (ε_r = 4.2), as a function of the substrate thickness, with the loss tangent as a parameter. These graphics, although obtained from the cavity model, make visible the behavior of the radiation efficiency of these microstrip antennas. Thus, if low-cost materials are used in the antenna manufacture, then moderately thick substrates must be adopted for good radiation efficiency. In the case of commercial FR4 laminates (ε_r = 4.2 and tan δ = 0.02), a radiation efficiency close to 70% can be obtained if a 6.5 mm thick antenna is designed.

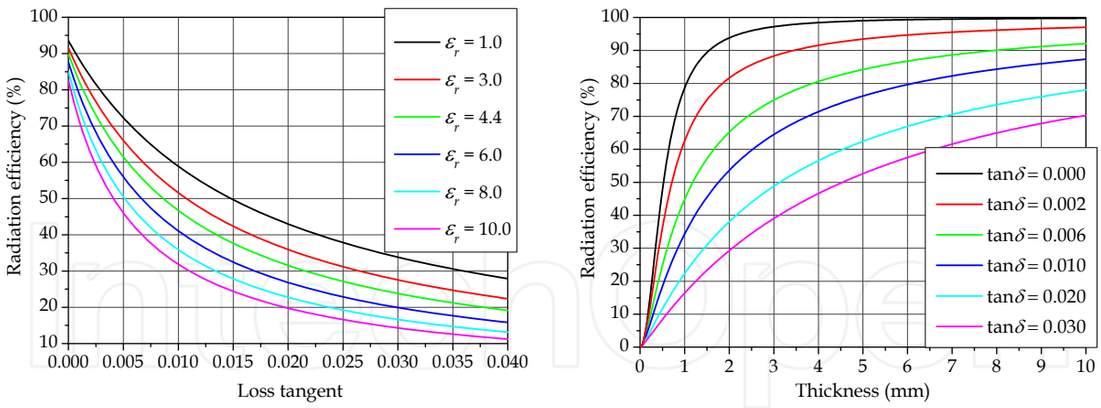

(a) (b)

Fig. 3. Radiation efficiency of LP microstrip antennas.

2.2 Rectangular patch: standard design

According to the standard procedure (James & Hall, 1989; Garg et al., 2001; Volakis, 2007) for designing a LP patch in the fundamental mode TM_{10}, the operating frequency is set up at the maximum input resistance point. Following this procedure and using the commercial software HFSS (HFSS, 2010) for optimizing the radiator dimensions, a rectangular antenna consisting of a h = 6.6 mm moderately thick (to obtain good radiation efficiency), FR4 (ε_r = 4.2 and tan δ = 0.02) substrate, fed by a 1.3-mm diameter coaxial probe, was designed to operate at 2 GHz. Utilizing a rectangular ground plane (L = 90 mm; W = 100 mm), the following optimal dimensions were obtained: a = 31.25 mm, b = 40.6 mm and p = 10.4 mm. Results for the input impedance and the reflection coefficient magnitude ($|\Gamma|$) are shown in Fig. 4(a) and (b) respectively. As expected, the radiation efficiency is 77.9% and the directivity is 7 dB at the operating frequency.

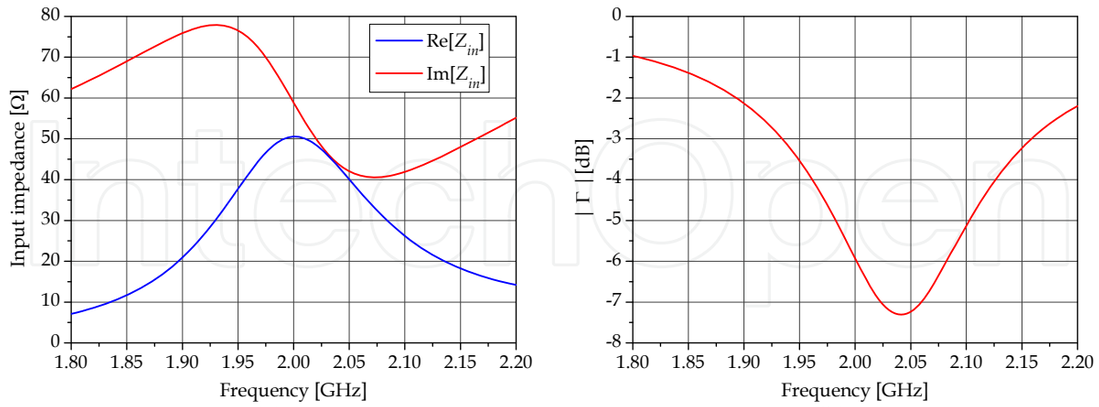

(a) (b)

Fig. 4. Standard design: (a) input impedance - (b) reflection coefficient magnitude.

It can be seen from Fig. 4(a) that the maximum input resistance occurs per design at the operating frequency (2 GHz). As a result, the antenna input impedance is highly inductive (Z_{in} = 50 + j59 Ω, at 2 GHz) and can not be perfectly matched to a 50-Ω SMA connector (i. e. $|\Gamma|$ = –6 dB, Fig. 4(b)) without an external network. Nowadays, this behavior is well known

and can be properly modeled by a parallel *RLC* network with a series inductance L_p (Richards et al., 1981). As a consequence, the radiator bandwidth is asymmetrical with respect to the operating frequency (Fig. 4(b)). To overcome this limitation, a new approach for designing probe-fed moderately thick microstrip antennas is proposed next.

2.3 Rectangular patch: new design

The new procedure, differently from the standard one, consists of designing the patch to operate at the zero input reactance X_{in} = 0 condition. This takes two steps; first, initial values for the patch dimensions are found, using the standard approach for example. Then, its feed probe is positioned close to the radiating edge ($p \cong 0$ mm). This action is performed to check if capacitive (i.e. negative reactance) input impedances can be reached at frequencies above the operating frequency (2 GHz), as shown in Fig. 5; if so, it is clear that the antenna could be perfectly matched to the 50-Ω SMA connector for a certain intermediate feed probe position, though at a frequency greater than the operating one.

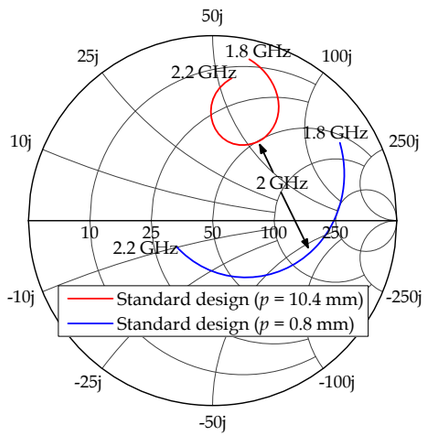

Fig. 5. Input impedances: standard design.

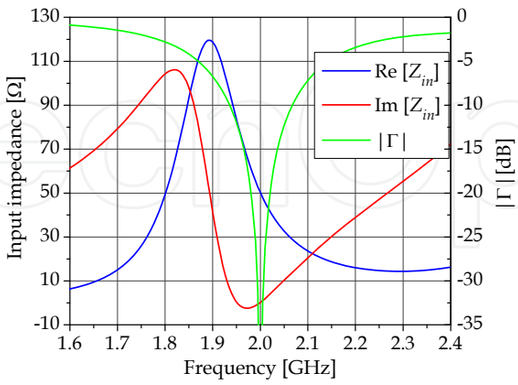

Fig. 6. Input impedance and reflection coefficient: new design.

To carry this out, starting from the initial patch dimensions, the probe position p is gradually reduced until the desired impedance is reached. The frequency where this happens can now be shifted down to the desired operating frequency through rescaling of the antenna geometry by increasing the patch dimensions (a and b). If on the other hand,

upon repositioning the probe close to the radiating edge the antenna input impedance remains inductive, a perfect match to the SMA connector may not be achieved, but even so a reflection coefficient that is better than the one obtained from the standard design can still be realized. This particular situation, which depends on the antenna thickness, substrate permittivity and the operating frequency, is not treated in this chapter.

Using the new approach, the antenna is redesigned to operate at 2 GHz for the same dielectric thickness, ground plane dimensions and probe diameter used in the standard design. The new optimized dimensions are: a = 32.9 mm, b = 42.8 mm and p = 7.0 mm. As expected, the new patch dimensions are now larger, whereas the new probe position is shorter, than their corresponding initial values. Results for the input impedance and the reflection coefficient magnitude of the new antenna are shown in Fig. 6. Now, the antenna matches perfectly the 50-Ω SMA connector and presents a symmetrical bandwidth with respect to the operating frequency (2 GHz). In addition, as observed in Fig. 6, the maximum resistance is greater than 50 Ω and occurs at a frequency below 2 GHz.

It is important to point out that the new method was conceived based on the properties of the antenna input impedance equivalent circuit (parallel *RLC* network with a series inductance L_p), typical of linearly-polarized probe-fed radiators. Consequently, this procedure is independent of the patch shape so it can be equally well applied to the design of other patch geometries, like the circular and the triangular ones.

2.4 Comparison between standard and new designs

To complete the analysis of the probe-fed patch antenna designed according to this new approach, it is important to verify the behavior of its radiation patterns. For this purpose, radiation patterns of the E_{theta} and E_{phi} components for both antennas (new and standard) are plotted on the *yz* and *xz* planes, as shown in Fig. 7(a) and (b). As noted, there are no significant differences between these patterns, even in the cross-polarization case. Besides, the directivity of the standard antenna is 7 dB whereas the new one is 7.1 dB. The new antenna efficiency is close to 79.1%.

This new design approach has been successfully used recently in (Tinoco S. et al., 2008) for designing thin microstrip antennas for educational purposes.

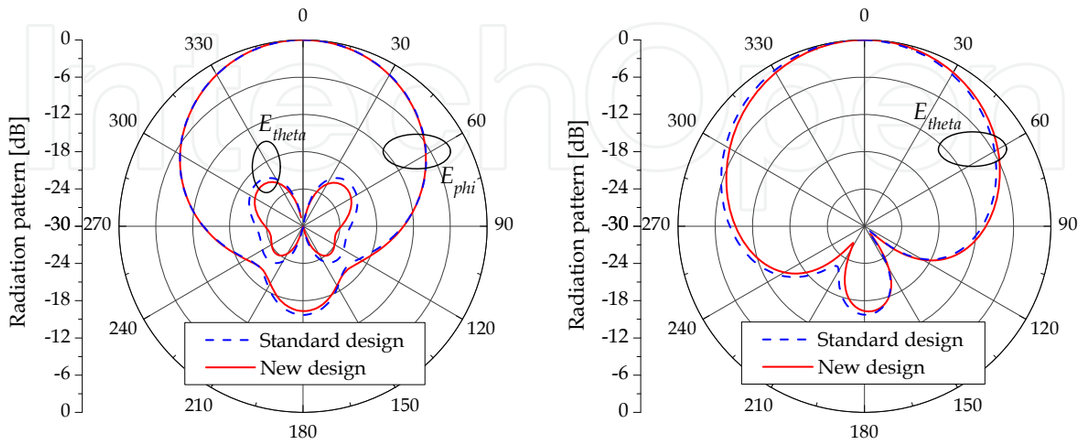

Fig. 7. Radiation patterns: (a) *yz* plane - (b) *xz* plane.

3. Circularly-polarized microstrip antennas

Singly-fed circularly-polarized microstrip antennas are largely employed in GPS receivers (Nascimento et al., 2006). Nearly-square and truncated-corner square patches (Figs. 8(a) and (b), respectively), have typically been used to obtain circular polarization (Garg et al., 2001). In this section, however, a new design approach is applied to the CP nearly-square patch. The geometry is given in Fig. 8(a), where a and b are its dimensions and p_x and p_y define the x and y coordinates of the probe position.

3.1 Nearly-square patch: standard design

Singly-fed rectangular CP microstrip antennas operate through a perturbation technique. The classical case is the rectangular thin radiator (James & Hall, 1989; Garg et al., 2001) that can be properly analyzed by means of an equivalent cavity model. According to this analysis, a CP nearly-square ($a \cong b$) radiator can be designed by feeding the patch along one of its diagonals. A left-hand CP radiation is obtained by positioning the probe along the dashed line illustrated in Fig. 8(a), were ($a > b$). For right-hand CP operation, the probe must be positioned along the other patch diagonal. A step-by-step design procedure is given in (Lumini et al., 1999).

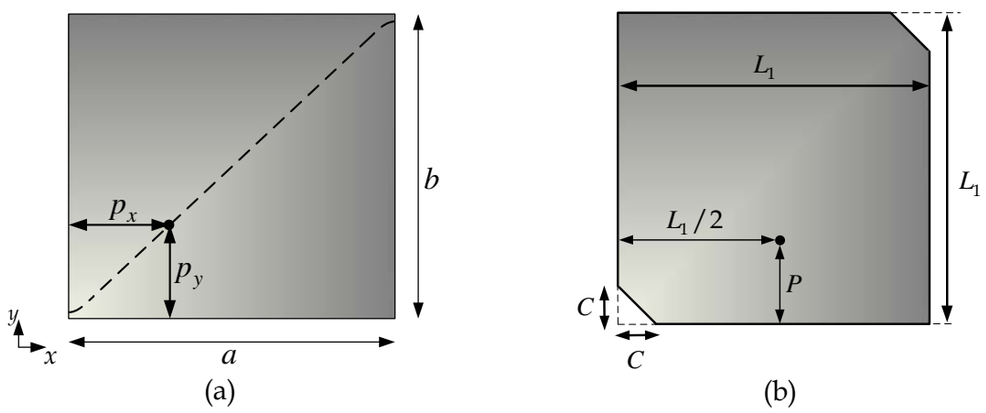

Fig. 8. Singly-fed CP microstrip patches: (a) nearly-square - (b) truncated-corner.

Based on this procedure and using HFSS for optimizing the antenna dimensions, a left-hand CP radiator with a moderately thick (6.6 mm) FR4 dielectric substrate (ε_r = 4.2 and $\tan\delta$ = 0.02), fed by a 1.3-mm diameter coaxial probe, was designed to operate at 2.5 GHz. Utilizing a finite square substrate and a 90-mm square ground plane, the following dimensions were obtained: a = 26.4 mm, b = 22.8 mm, p_x = 9.95 mm and p_y = 7.9 mm. Results for the input impedance are shown in Fig. 9(a).

As expected, the operating frequency occurs between the fundamental TM_{10} and TM_{01} modes, each one corresponding to the input resistance maxima (at 2.39 GHz and 2.6 GHz, respectively). As a consequence, its input impedance is highly inductive (Z_{in} = 50 + j60 Ω) at the operating frequency (2.5 GHz) and the antenna is not properly matched to the 50-Ω SMA coaxial connector. Since the radiator under consideration exhibits an asymmetrical bandwidth, the best axial ratio (calculated in the broadside region) and the best reflection coefficient magnitude occur at different frequencies, as shown in Fig. 9(b).

The equivalent circuit shown in Fig. 10 (James & Hall, 1989) for singly-fed CP microstrip antennas can be used for better characterization of the mismatch problem. Taking this circuit into account, curves for the impedances (Z_{in1} and Z_{in2}) of each individual fundamental mode are presented in Fig. 11. At the operating frequency, however, the condition $n_1 = n_2 = 1$ must be satisfied. In this situation, the equivalent circuit is simplified and the following identities $\mathrm{Im}[Z_{in1}] = -\mathrm{Im}[Z_{in2}]$ and $\mathrm{Re}[Z_{in1}] = \mathrm{Re}[Z_{in2}]$ are verified. Consequently, at the operating frequency, the antenna input reactance is given only by the (inductive) reactance of the probe (L_p). Besides, frequencies f_1 and f_2 are tied up to the dimensions a and b, respectively, and the amplitude of the modes to the probe positions p_x and p_y.

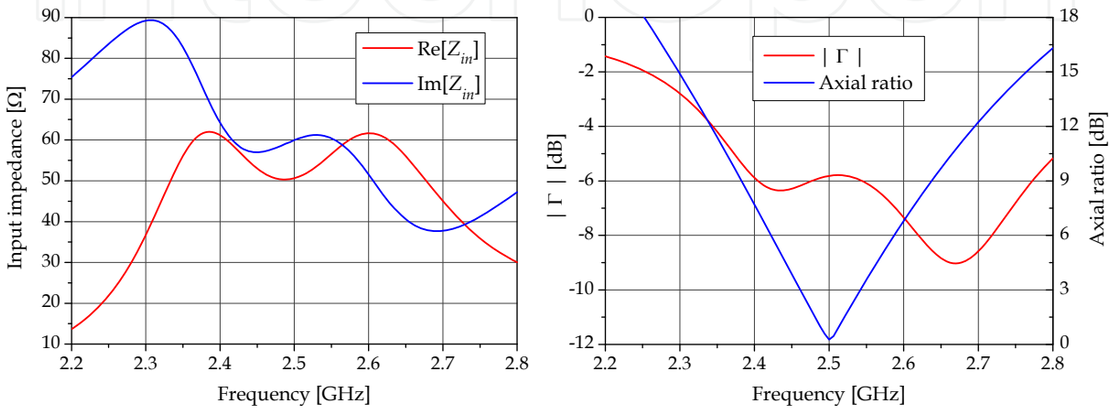

Fig. 9. Singly-fed CP microstrip patch: (a) input impedance - (b) axial ratio and reflection coefficient magnitude.

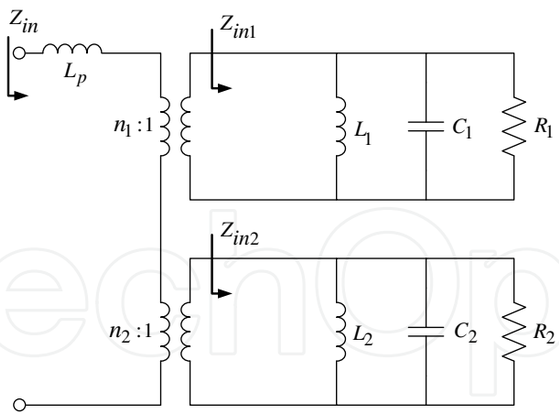

Fig. 10. Equivalent circuit for singly-fed CP microstrip antennas.

To overcome the aforementioned limitations, an innovative approach for designing singly-fed CP patch antennas is presented next. The goal is to get the best axial-ratio and $|\Gamma|$ both at the same frequency.

3.2 Rectangular patch: new design

The new strategy starts from a rectangular patch ($a \neq b$), instead of a nearly-square ($a \cong b$) one, and aims at establishing a capacitive reactance from the combination of the reactances

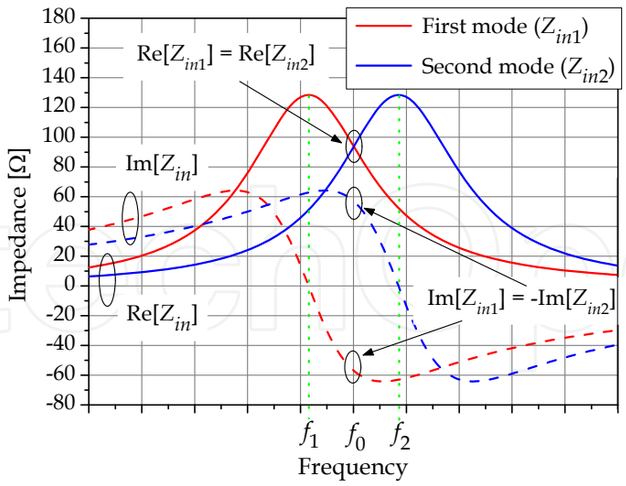

Fig. 11. Impedances of the fundamental modes: standard design.

of the two fundamental TM_{10} and TM_{01} modes at the frequency where Re[Z_{in1}] = Re[Z_{in2}]. This capacitive reactance is then used to compensate for the probe's inductive reactance, resulting in an excellent matching with the SMA coaxial connector (of 50-Ω characteristic impedance in the present case). This situation is shown in Fig. 12.

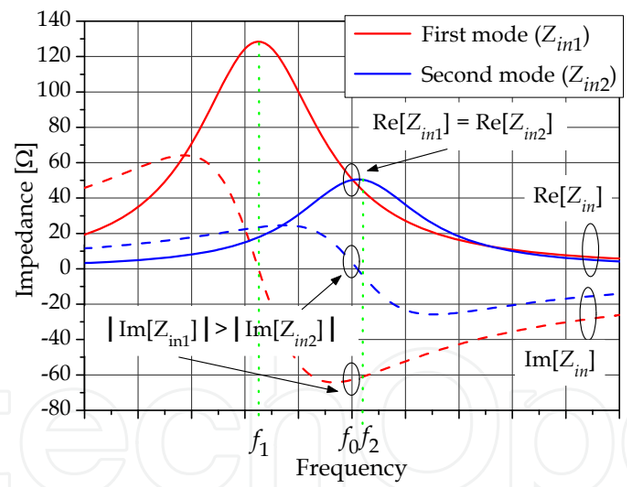

Fig. 12. Impedances of the fundamental modes: new design.

Compared with the standard approach, one notes that frequencies f_1 (of the first mode) and f_2 (of the second mode) are both shifted down. Frequency f_2 is now positioned near the operating frequency (2.5 GHz) and the amplitude of the first mode is greater than that of the second one. As a consequence, the new patch dimensions will be larger than those from the standard design, whereas the probe position p_x is reduced while p_y increases, under the conditions ($a > b$) and ($p_x < a/2$). On the other hand, if ($a > b$) and ($p_x > a/2$), then p_x increases while p_y is reduced. But before proceeding, a critical question needs to be posed at this point: can the proposed geometry establish CP radiation at the frequency where the antenna input impedance is purely real?

To answer this question, modifications in the standard design approach (Lumini et al., 1999) for nearly-square ($a \cong b$) patches were performed to encompass the present situation ($a \neq b$). As a result, a new feed locus equation, given by (6), is obtained for CP operation

$$p_y = \frac{b}{\pi}\cos^{-1}\left(\frac{2B\cos(\pi p_x / a)}{C\Delta \pm \sqrt{-4C^2B^2 + C^2\Delta^2}}\right), \tag{6}$$

where

$$C = \frac{b}{a}\mathrm{sinc}[\pi(a-b)/(2a)], \tag{7}$$

$$\Delta = \pi(b^{-1} - a^{-1}), \tag{8}$$

$$B = k_d(\delta_{ef}/2), \tag{9}$$

$$k_d = \omega\sqrt{\mu_0\varepsilon_0\varepsilon_r}, \tag{10}$$

δ_{ef} is the antenna effective loss tangent and $\mathrm{sinc}(x) = \sin(x)/(x)$.

In the standard design δ_{ef} is calculated as an intermediate value between the effective loss tangent of the first and the second fundamental modes. Instead, as in the new approach frequency f_2 is close to the operating frequency f_0, the value of δ_{ef} can now be approximated by that calculated at f_2 only.

The positive sign before the square root in (6) results in the dashed line shown in Fig. 13. From this figure, one can see that the feed locus does not fall upon the patch diagonal as in the standard design, behaving as predicted in (Engest & Lo, 1985). Consequently, p_x must be reduced and p_y increased (if $p_x < a/2$), in comparison to the standard design. Thus, by positioning the probe along the aforementioned dashed line, such left-hand circular polarization antenna can be matched to the SMA connector.

On the other hand, if the negative sign before the square root in (6) is taken into account, the probe position p_x increases while p_y is reduced (if $p_x < a/2$). In this case, the antenna input impedance becomes more inductive and the proposed approach can not be applied.

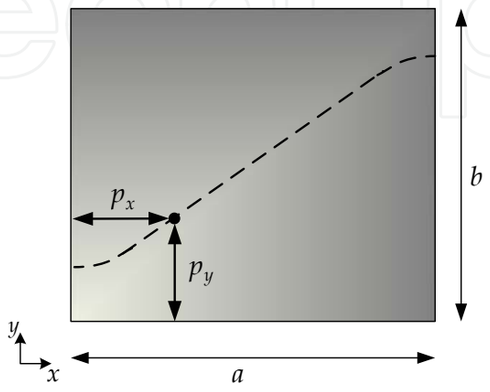

Fig. 13. Singly-fed CP rectangular patch.

To exemplify the application of the proposed strategy, a new left-hand CP antenna is designed to operate at 2.5 GHz with the same substrate characteristics, ground plane dimensions and probe diameter specified in the former design. As in the LP case, the HFSS software is used for optimizing the antenna dimensions. Consequently, it is necessary to set up the initial patch dimensions as well as the probe coordinates. In this chapter, the standard design dimensions and the coordinates given by (6) were used as the starting point.

The next step is the optimization of the probe position such that Re[*Zin*] = 50 Ω at the operating frequency (f_0) and the best axial ratio point occurs as close as possible to this frequency. In order to simultaneously obtain the best axial ratio and $|\Gamma|$ at f_0, the optimization procedure depends on each of the following conditions, where f_r denotes the best axial ratio frequency:

- If Im[Z_{in}] > 0 at f_0, and $f_r > f_0$, then both antenna dimensions and their ratio (a/b) must be increased.
- If Im[Z_{in}] > 0 at f_0, and $f_r < f_0$, then the antenna dimensions must be reduced whereas the ratio (a/b) must be increased.
- If Im[Z_{in}] > 0 at f_0, and $f_r = f_0$, then the ratio (a/b) must be increased, but reducing b and increasing a in the same proportion.
- If Im[Z_{in}] < 0 at f_0, and $f_r > f_0$, then the antenna dimensions must be increased whereas the ratio (a/b) must be reduced.
- If Im[Z_{in}] < 0 at f_0, and $f_r < f_0$, then both antenna dimensions and their ratio (a/b) must be reduced.
- If Im[Z_{in}] < 0 at f_0, and $f_r = f_0$, then the ratio (a/b) must be reduced, but increasing b and reducing a in the same proportion.
- If Im[Z_{in}] = 0 at f_0, and $f_r > f_0$, then both antenna dimensions and their ratio (a/b) must be increased.
- If Im[Z_{in}] = 0 at f_0, and $f_r < f_0$, then both antenna dimensions and their ratio (a/b) must be reduced.

After this procedure, the following dimensions were obtained: a = 28.25 mm, b = 23.60 mm, p_x = 6.00 mm and p_y = 8.10 mm. Results for the input impedance are presented in Fig. 14(a). The value of the antenna input impedance at the operating frequency is now purely 50 Ω. Graphics for the axial ratio and the reflection coefficient magnitude are depicted in Fig. 14(b).

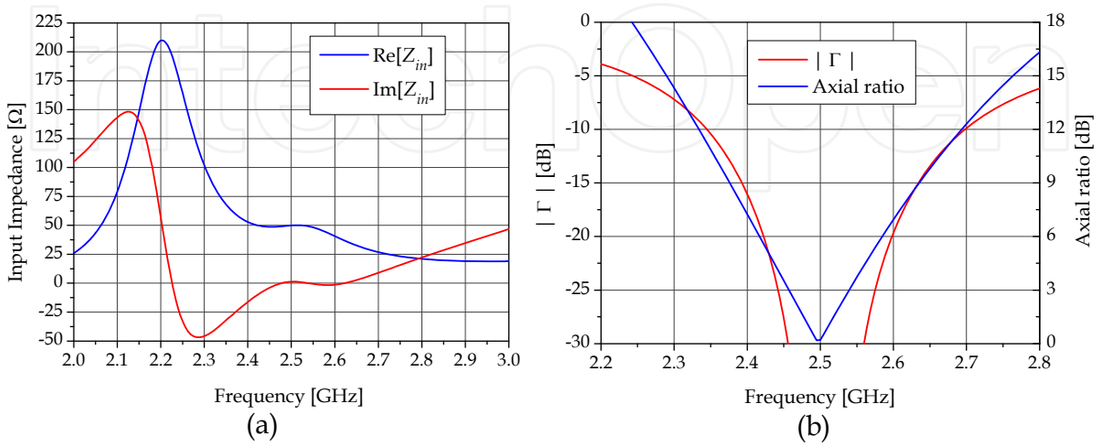

Fig. 14. Rectangular patch: (a) input impedance - (b) axial ratio and reflection coefficient magnitude.

One can see from these figures that the design goals were reached: both curves exhibit their best values right around the operating frequency. For verification purposes, Fig. 15 presents the feed locus plotted on the antenna patch, based on the data in Table 1. As expected, this confirms the behavior illustrated in Fig. 13.

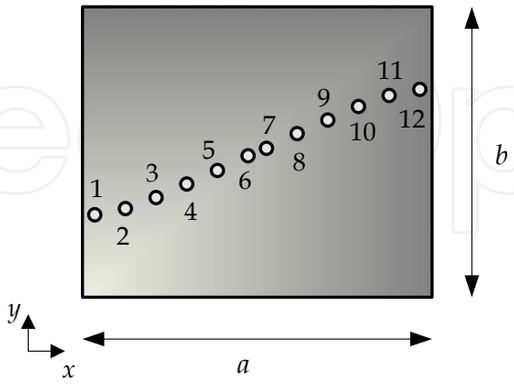

Fig. 15. Feed locus for CP antenna: new design.

	p_x (mm)	p_y (mm)
1	1.00	6.70
2	3.50	7.20
3	6.00	8.10
4	8.50	9.20
5	11.00	10.30
6	13.50	11.50
7	15.00	12.10
8	17.50	13.30
9	20.00	14.40
10	22.50	15.50
11	25.00	16.40
12	27.50	16.90

Table 1. Probe position for CP operation: new design.

The applicability of this new approach depends on the substrate thickness. In case of electrically thicker antennas, the proposed approach may fail since the feed locus deviates from the patch diagonal, tending to be parallel to the x-axis, if $a > b$. Besides, the probe position must be moved toward the antenna edge ($p_x \cong 0$ mm) for matching the antenna to a SMA connector.

3.3 Comparison between standard and new designs

To complete the analysis of the singly-fed CP antenna designed according to the new approach, its radiation patterns are now considered. Graphics of its E_{theta} and E_{phi} components on the yz and xz planes are compared to those from the antenna designed following the standard procedure in Figs. 16-17.

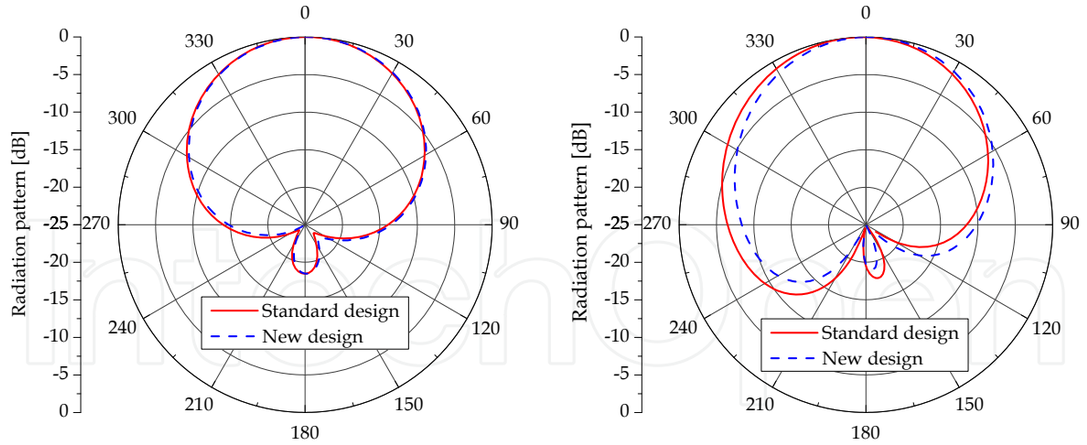

Fig. 16. Radiation patterns in *xz* plane: (a) E_{phi} component - (b) E_{theta} component.

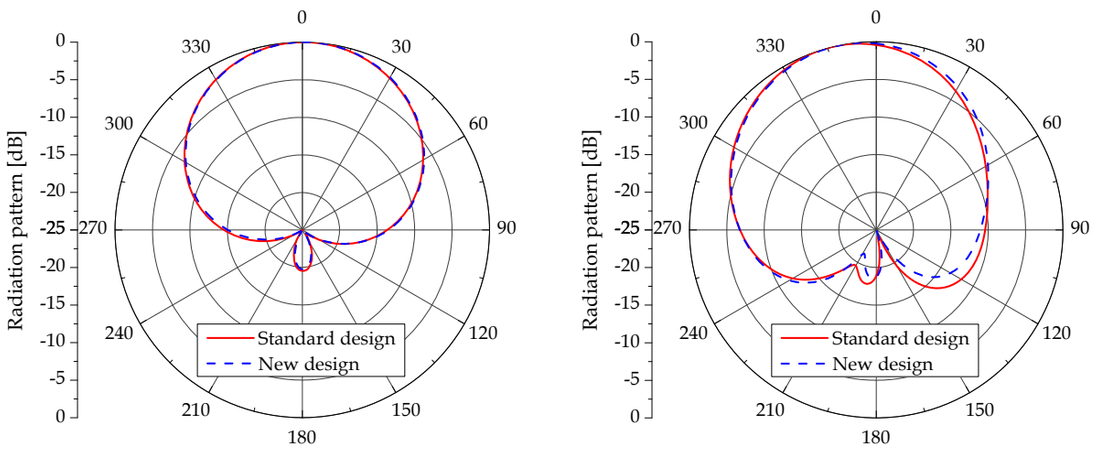

Fig. 17. Radiation patterns in *yz* plane: (a) E_{phi} component - (b) E_{theta} component.

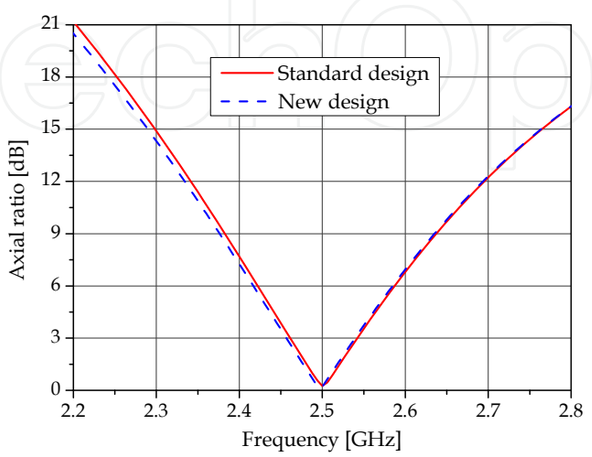

Fig. 18. Axial ratio comparison.

As seen, there are no significant differences between these patterns. Besides, the directivities are 6.6 dB for the nearly-square antenna and 6.8 dB for the new design. Although moderately thick, the antennas' efficiencies are 79.1% for nearly-square and 79.7% for the new design. The behavior of their axial ratios can be observed in Fig. 18.

4. Prototypes

To gather experimental confirmation of the effectiveness of the abovementioned new strategies, two prototypes, one linearly and the other circularly polarized, were designed, manufactured and tested using the FR4 substrate specified in this chapter.

4.1 Linearly polarized microstrip antenna

The geometry of the LP antenna designed to operate at 2 GHz is presented in Fig. 1. The following dimensions were calculated in Section 2.3 (a = 32.9 mm, b = 42.8 mm and p = 7.0 mm). A photo of the prototype is shown in Fig. 19.

Fig. 19. Photo of the LP microstrip antenna prototype.

Experimental results for the input impedance and the reflection coefficient magnitude are presented in Figs. 20(a) and (b). As seen, they are in excellent agreement with the HFSS simulation, thus validating the newly proposed design strategy for LP radiators.

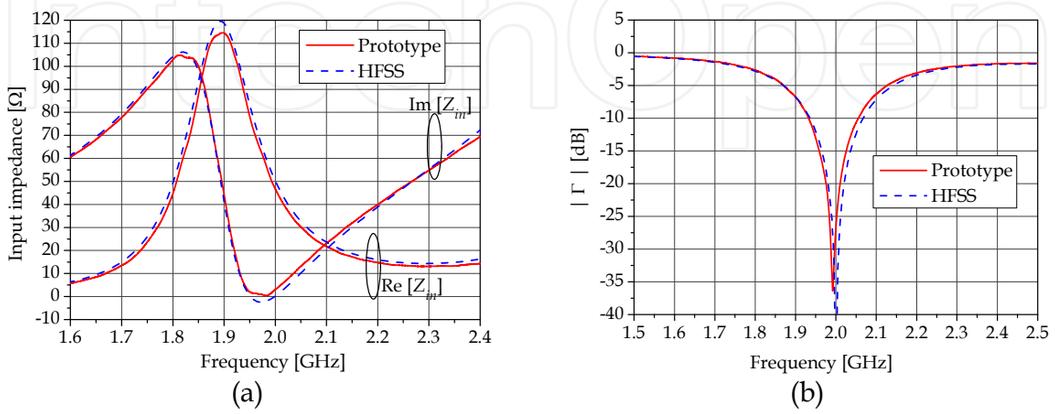

Fig. 20. LP microstrip antenna: (a) input impedance - (b) reflection coefficient magnitude.

4.2 Circularly-polarized microstrip antenna

The geometry of the CP antenna designed to operate at 2.5 GHz is presented in Fig. 13. The following dimensions were calculated in Section 3.2 (a = 28.25 mm, b = 23.60 mm, p_x = 6.00 mm and p_y = 8.10 mm). A photo of the prototype is shown in Fig. 21.

Fig. 21. Photo of the CP microstrip antenna prototype.

Experimental results for the input impedance and the reflection coefficient magnitude are presented in Figs. 22(a) and (b), and for the broadside axial ratio in Fig. 23. As seen, they are in very good agreement with HFSS simulations.

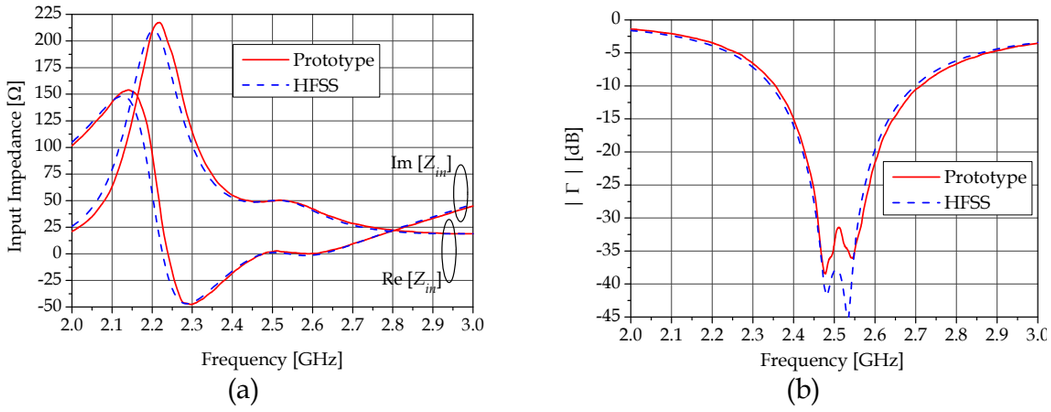

Fig. 22. CP microstrip antenna: (a) input impedance - (b) reflection coefficient magnitude.

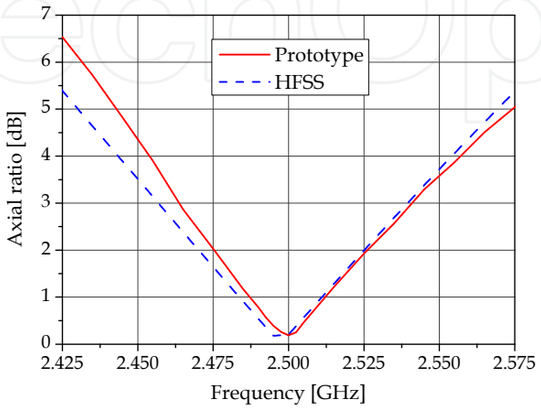

Fig. 23. Axial ratio comparison.

5. Other applications

As previously mentioned the new method was conceived based on the behavior of the input impedance of LP and CP antennas. Consequently, this procedure can be applied to the design of other patch geometries since their input impedance can be represented by the same equivalent circuit. Moreover, the method is not restricted to low-cost substrates, applying equally well to the design of LP or CP microstrip patches printed on any moderately thick commercial microwave laminates. These cases are discussed next.

5.1 Linearly polarized microstrip antennas

Different patch geometries are used nowadays to radiate LP electromagnetic waves (James & Hall, 1989; Garg et al., 2001; Volakis, 2007). Among them, the circular and PIFA radiators, since their input impedance can be represented by the same equivalent circuit used for rectangular antennas, were chosen to exemplify the application of the new proposed procedure in the case of a typical low-loss microwave laminate (ε_r = 2.55 and tan δ = 0.0022).

5.1.1 Circular patch

In the first application, a moderately thick (h = 6.35 mm) LP circular patch was designed to operate at 2.85 GHz using the HFSS software. The antenna geometry and dimensions are presented in Fig. 24(a). A photo of the prototype is shown in Fig. 24(b).

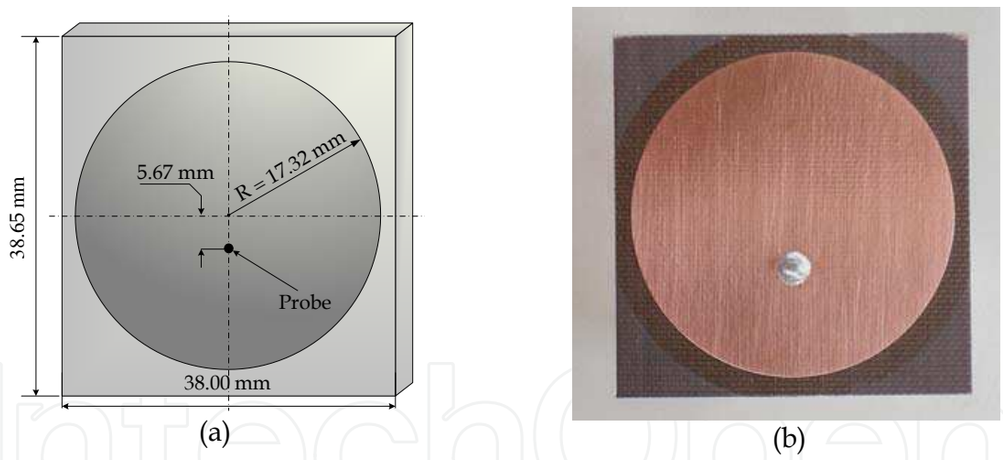

Fig. 24. LP circular patch: (a) geometry - (b) photo of the prototype.

Results for the input impedance and reflection coefficient magnitude are presented in Figs. 25(a) and (b), respectively. Very good agreement is observed between the simulated and measured results.

5.1.2 PIFA antenna

In the second application, the focus is on the planar inverted F antenna (PIFA), a well know topology used for LP antennas of reduced dimensions (Chen et al., 2005). Following (Tinoco S. et al., 2008), an electrically thin antenna with h = 3.048 mm of substrate thickness was designed to operate near 2 GHz, using the HFSS software. The antenna geometry and dimensions are presented in Fig. 26(a). A photo of the prototype is shown in Fig. 26(b).

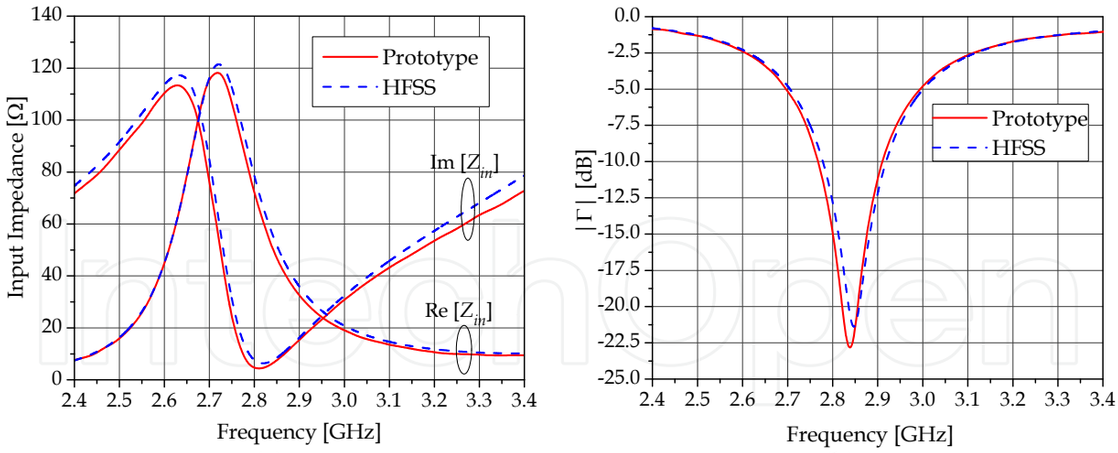

Fig. 25. LP circular patch: (a) input impedance - (b) reflection coefficient magnitude.

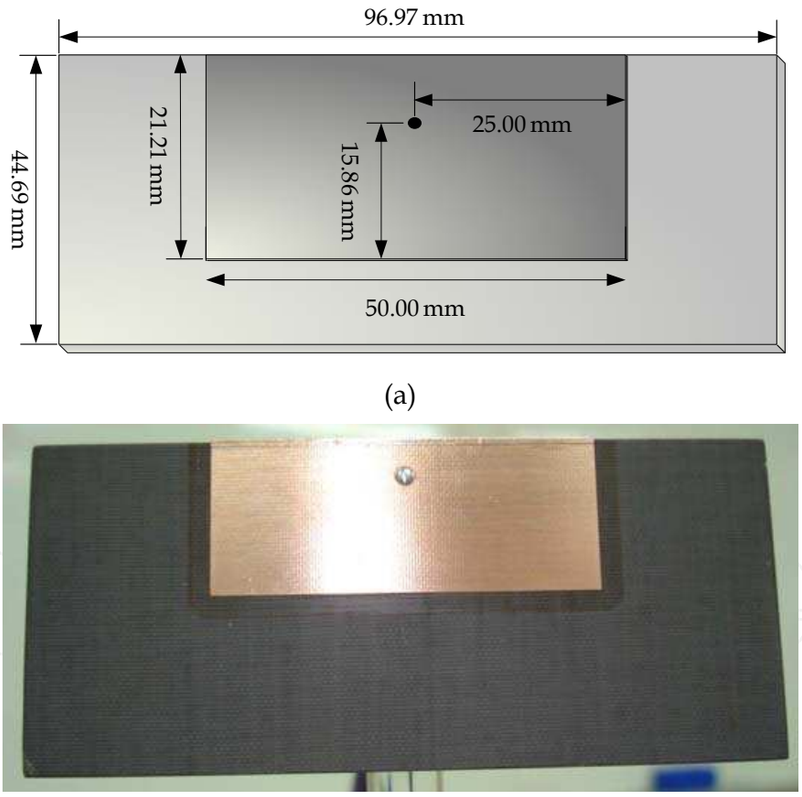

Fig. 26. PIFA antenna: (a) geometry - (b) photo of the prototype.

Results for the input impedance and reflection coefficient magnitude are presented in Figs. 27(a) and (b) respectively. Once again, very good agreement is observed between simulated and measured results.

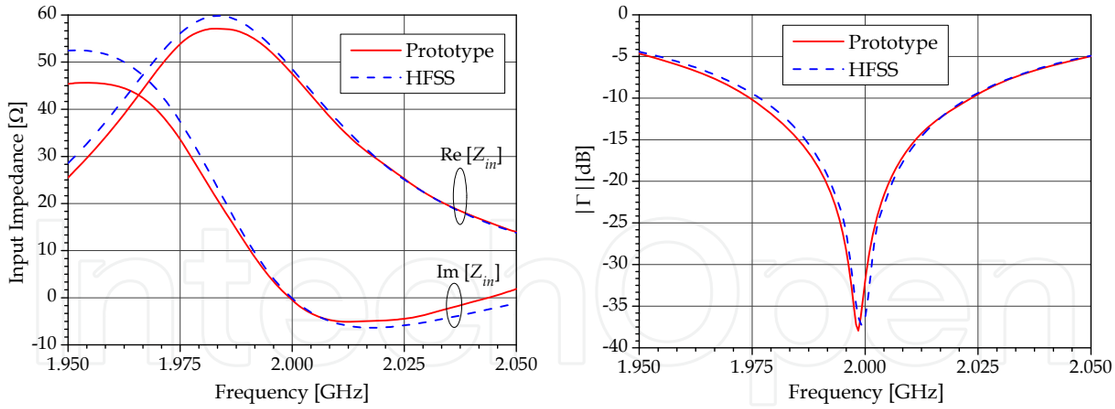

Fig. 27. PIFA antenna: (a) input impedance - (b) reflection coefficient magnitude.

5.2 Circularly-polarized microstrip antennas

Truncated corner probe-fed microstrip antennas can be designed to operate at the zero input reactance X_{in} = 0 condition, since their input impedance can be represented by the same equivalent circuit used for nearly-square radiators. To illustrate the applicability of this condition, two CP antennas are analyzed; one designed to meet specific requirements of Glonass applications and other to comply with the Globalstar system.

5.2.1 Glonass antenna

For Glonass applications, receiver antennas have to be right-hand circularly polarized over an operating range from 1.598 to 1.609 GHz (Nascimento et al., 2008). In order to obtain an excellent matching at the same frequency of best axial ratio, the standard truncated-corner square patch will not work, so a rectangular antenna design (Nascimento et al., 2007b) is used.

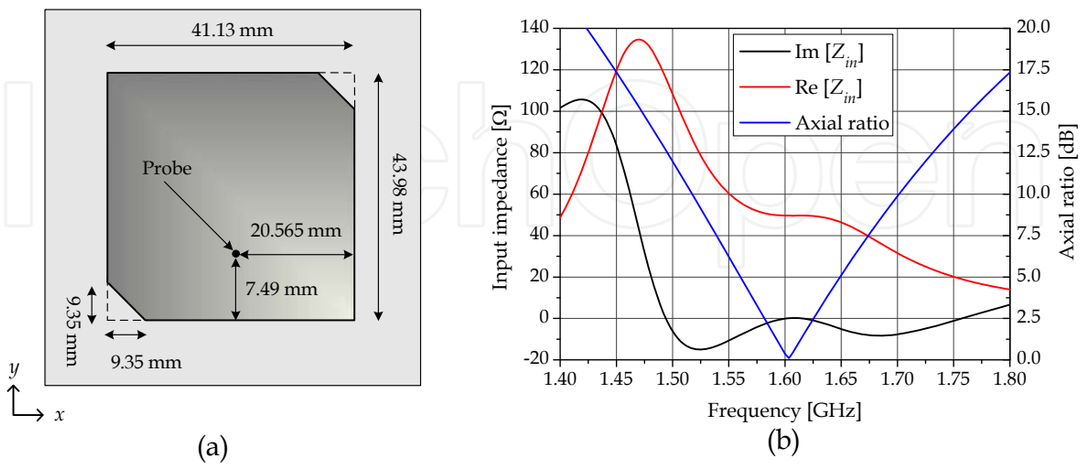

Fig. 28. CP truncated-corner patch: (a) geometry - (b) axial ratio and input impedance.

Following (Nascimento & Lacava, 2009), the truncated-corner rectangular patch (TCRP) illustrated in Fig. 28(a), printed on a finite FR4 substrate (ε_r = 4.4, tan δ = 0.02 and h = 6.6 mm)

and a 75-mm square ground plane was designed using the HFSS software for operation at 1.603 GHz. The optimized antenna dimensions are shown in Fig. 28(a), the simulated input impedance and axial ratio results are presented in Fig. 28(b) and the reflection coefficient magnitude in Fig. 29. As expected, the microstrip antenna with the new geometry exhibits very good AR (0.1 dB) and reflection coefficient magnitude (-48 dB) characteristics at 1.603 GHz, without the need for any external matching network.

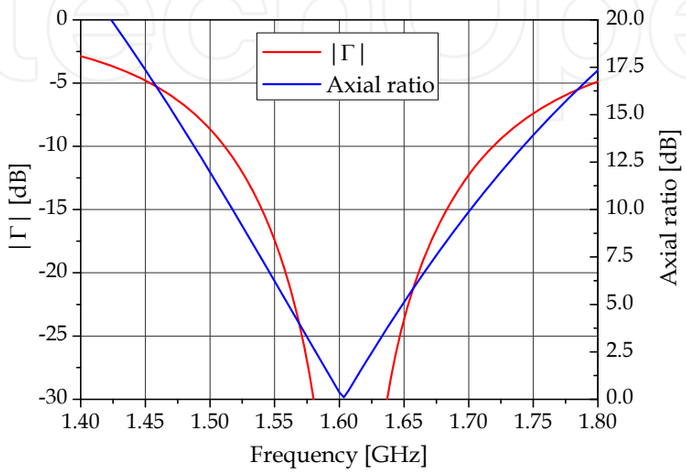

Fig. 29. CP truncated-corner patch: axial ratio and reflection coefficient magnitude.

5.2.2 Globalstar Antenna

Moderately thick microstrip antennas can also be used for bandwidth improvement. To exemplify such application a prototype of a Globalstar antenna was manufactured using a low-loss substrate (ε_r = 2.55, $\tan\delta$ = 0.0022 and h = 4.572 mm). Left-handed CP Globalstar mobile-terminals require two radiators. The first is designed for uplink frequencies (Tx - 1.61073 to 1.62549 GHz) while the other receives the downlink ones (Rx - 2.48439 to 2.49915 GHz) (Nascimento et al., 2007a). The antenna geometry and a photo of the prototype are shown in Figs. 30(a) and (b), respectively.

The optimized antenna dimensions (using the HFSS software) are presented on Table 2 for the radiators designed on finite ground plane and dielectric (L = 140 mm; W = 85 mm).

Tx		*Rx*	
L_{T1}	54.90 mm	L_{R1}	34.40 mm
L_{T2}	55.90 mm	L_{R2}	35.85 mm
C_T	7.55 mm	C_R	5.75 mm
P_T	15.85 mm	P_R	9.00 mm
D_T	71.00 mm	D_R	15.00 mm

Table 2. Globalstar antenna dimensions.

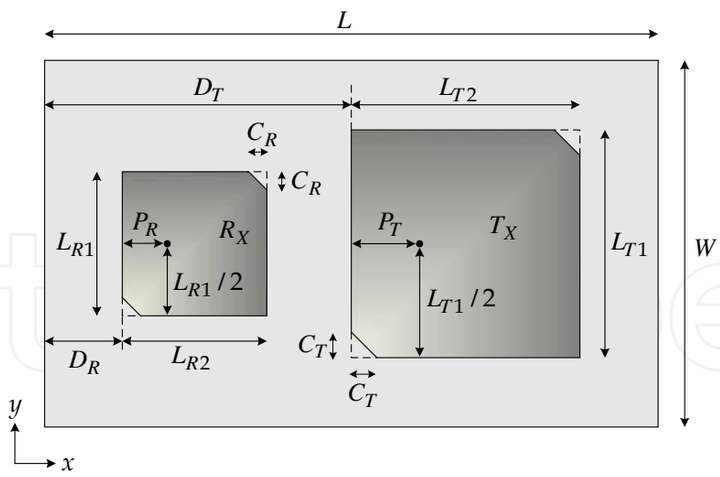

(a)

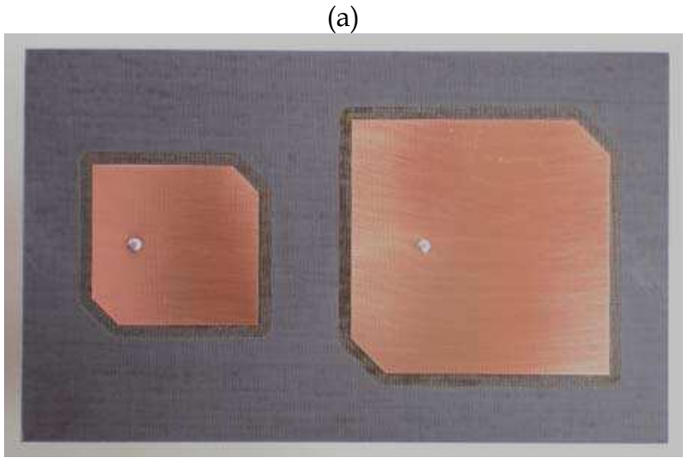

(b)

Fig. 30. Globalstar antenna: (a) geometry - (b) photo of the prototype.

The axial ratio and reflection coefficient magnitude are presented in Figs. 31 and 32 for the Tx and Rx antennas, respectively.

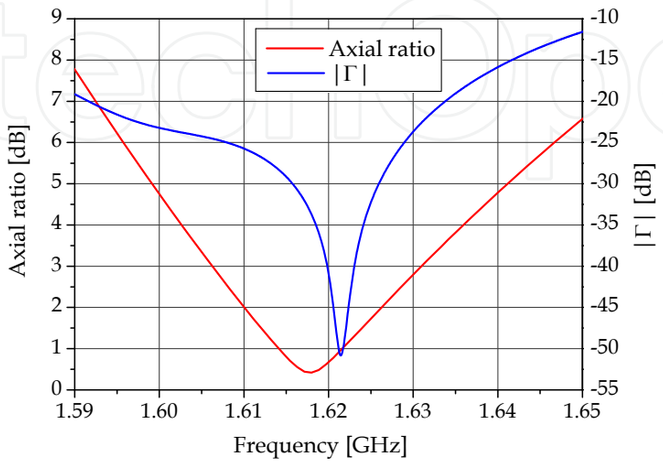

Fig. 31. Globalstar antenna axial ratio and reflection coefficient magnitude: Tx radiator.

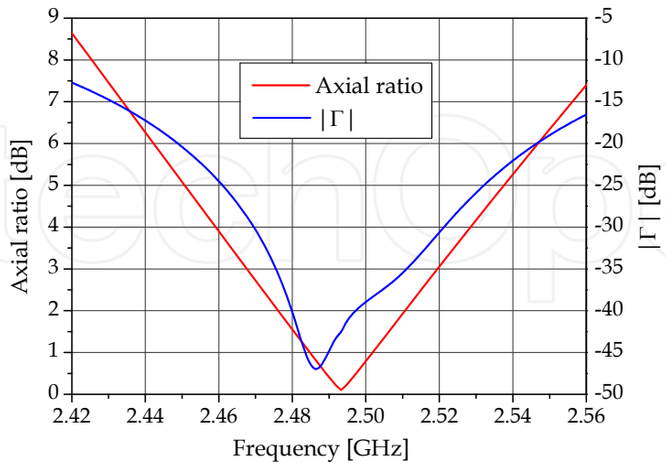

Fig. 32. Globalstar antenna axial ratio and reflection coefficient magnitude: Rx radiator.

Results for the input impedance on the Smith chart are presented in Figs. 33 and 34 for the Tx and Rx antennas, respectively. These results indicate that the antenna meets the Globalstar specifications.

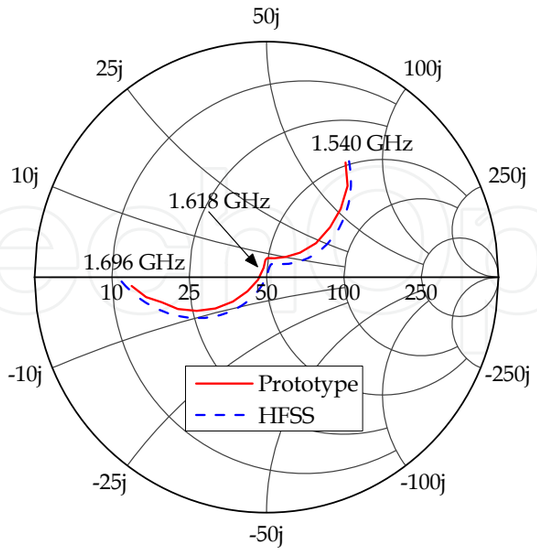

Fig. 33. Globalstar antenna input impedance: Tx radiator.

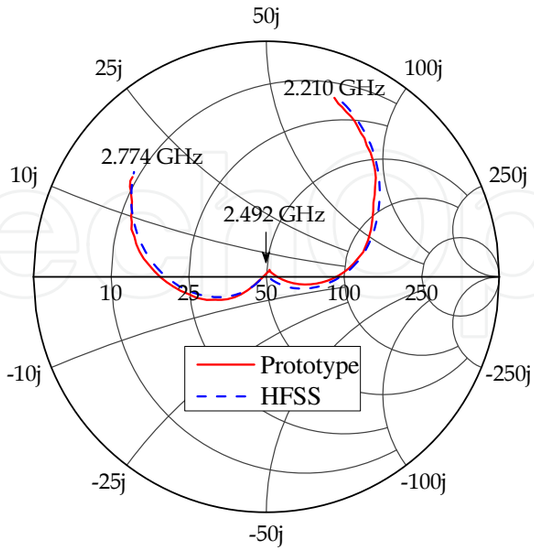

Fig. 34. Globalstar antenna input impedance: Rx radiator.

5.3 CP antenna radiation efficiency measurements

The radiation efficiency of a LP microstrip antenna can be efficiently measured using the Wheeler cap (Choo et al., 2005; Pozar & Kaufman, 1988; Sona & Rahmat-Samii 2006). According to Wheeler, the radiation resistance of an antenna can be separated from its loss resistance by enclosing the antenna with a radiation shield cap placed at a distance greater than $\lambda/(2\pi)$ (Wheeler, 1959). Consequently, since a linearly-polarized microstrip antenna can be modeled as a parallel *RLC* circuit, its efficiency is calculated by

$$\eta = \frac{G_{out} - G_{cap}}{G_{out}}, \tag{11}$$

where G_{cap} is the conductance of the admittance measured with the cap in place and G_{out} is the conductance of the admittance measured with the cap removed.

In the case of a CP microstrip antenna an innovative radiation efficiency analysis using the Wheeler cap method was presented in (Nascimento & Lacava, 2009). This procedure is discussed next, for the case of the Glonass antenna designed in Section 5.2.1.

Differently from the standard design, the two orthogonal resonant modes in the new approach are now asymmetrically positioned in relation to the frequency for optimal axial ratio as presented in Fig. 28 (b). In addition, at the lower resonant frequency (1.468 GHz), its 15.45-dB axial ratio shows the antenna tends to be linearly polarized around this frequency. This result supports the use of the Wheeler cap method for measuring the antenna radiation efficiency at this frequency.

The cap geometry is shown in Fig. 35 where the radiator is positioned inside a cubic cavity of electrically conducting walls of 270-mm internal dimension.

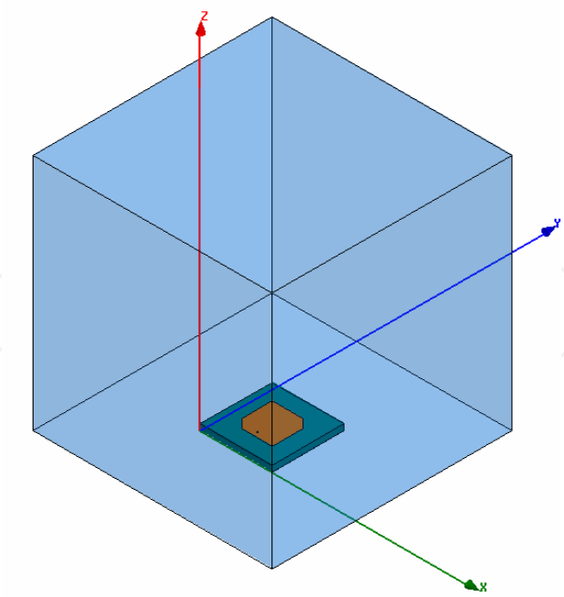

Fig. 35. Geometry of the Wheeler cap simulation through the HFSS package.

HFSS simulation results for the real part of the input impedance are presented in Fig. 36, both with and without the cubic cavity. Making use of equation (11) for the lower resonant mode (G_{cap} = 1.92 mS and G_{out} = 7.43 mS), the radiation efficiency computed from the Wheeler method is 74.16%. The free-space radiation efficiency, computed with the HFSS package is 74.68% at 1.468 GHz, which is only 0.7% off. Consequently, the Wheeler cap method can be used for accurately determining the radiation efficiency of TCRP radiators.

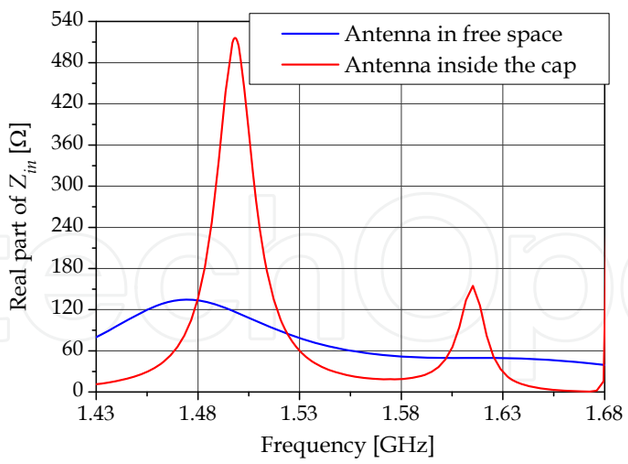

Fig. 36. Low-cost Glonass antenna: real part of its input impedance.

6. Conclusion

In this chapter, new effective strategies for designing probe-fed moderately thick LP and CP microstrip antennas were presented. As the design procedures do not make use of external networks, the antenna construction process is considerably simplified. Besides, as the new

methodologies are based on properties of the antenna equivalent circuit, they can be applied to the design of microstrip radiators of arbitrary patch shapes. Moreover, it is not restricted to low-cost substrate thus applying equally well to the design of LP or CP microstrip patches printed on any moderately thick commercial microwave laminates. Experimental results for LP and CP radiators validate the design strategies for both the LP and CP cases. Moreover, the Wheeler cap method is shown to be an effective means for simulating the radiation efficiency of CP microstrip antennas.

The excellent practical results obtained when matching microstrip patch radiators to a 50-Ω SMA connector can be readily extended to the synthesis of inductive or capacitive input impedances, as for example in the case of optimization of the noise figure and stability of low-noise power amplifiers connected directly to the antenna. Another possible application is the design of low-cross-polarization probe-fed microstrip arrays (Marzall, et al., 2009; Marzall et al., 2010).

7. References

Alexander, M. J. (1989). Capacitive matching of microstrip antennas. *IEE Proceedings of Microwaves, Antennas and Propagation*, Vol. 137, No. 2, (Apr. 1989) (172-174), ISSN: 0950-107X.

Chang, F. S. & Wong, K. L. (2001), A broadband probe-fed patch antenna with a thickened probe pin, *Proceedings of Asia-Pacific Microwave Conference*, (1247-1250), ISBN: 0-7803-7138-0, Taipei, China, Dec. 2001

Chen, H. M.; Lin, Y. F.; Cheng, P. S.; Lin, H. H.; Song, C. T. P. & Hall, P. S. (2005), Parametric study on the characteristics of planar inverted-F antenna. *IEE Proceedings of Microwaves, Antennas and Propagation*, (Dec. 2005) (534-538), ISSN: 1350-2417.

Choo, H.; Rogers, R. & Ling, H. (2005), Comparison of three methods for the measurement of printed antennas efficiency, *IEEE Transactions on Antennas and Propagation*, Vol. 53, No. 7, (Jul. 2005) (2328-2332), ISSN: 0018-926X.

Dahele, J. S.; Hall, P. S. & Haskins, P. M. (1989), Microstrip patch antennas on thick substrates, *Proceedings of Antennas and Propagation Society International Symposium*, pp. 458-462, San Jose, CA, USA, Jun. 1989.

Engest, B. & Lo, Y. T. (1985), A study of circularly polarized rectangular microstrip antennas, *Technical Report*, Electromagnetics Laboratory, University of Illinois.

Gardelli, R.; La Cono, G. & Albani, M. (2004), A low-cost suspended patch antenna for WLAN access points and point-to-point links, *IEEE Antennas and Wireless Propagation Letters,* Vol. 3, (2004) (90-93), ISSN: 1536-1225.

Garg, R.; Bhartia, P.; Bahl, I. & Ittipiboon, A. (2001). *Microstrip Antenna Design Handbook*, Artech House, ISBN: 0-89006-513-6, Boston.

Hall, P. S. (1987). Probe compensation in thick microstrip patches. *Electronics Letters,* Vol. 23, No. 11, (May 1987) (606-607), ISSN: 0013-5194.

Haskins, P. M. & Dahele, J. S. (1998), Capacitive coupling to patch antenna by means of modified coaxial connectors, *Electronics Letters*, Vol. 34, No. 23, (Nov. 1998) (2187-2188), ISSN: 0013-5194.

HFSS (2010), Product overview, *Available: http://www.ansoft.com/products/hf/hfss/*, (Sept. 2010).

IEEE Std 145 (1993). *IEEE Standard Definitions of Terms for Antennas*, ISBN: 1-55937-317-2, New York, USA.

James, J. R. & Hall, P. S. (1989). *Handbook of Microstrip Antennas*, Peter Peregrinus, ISBN: 0-86341-150-9, London.

Lee , K. F. & Chen, W. (1997). *Advances in Microstrip and Printed Antennas*, John Wiley, ISBN: 0-471-04421-0, New York.

Lumini, F.; Cividanes, L. & Lacava, J. C. S. (1999), Computer aided design algorithm for singly fed circularly polarized rectangular microstrip patch antennas, *International Journal of RF and Microwave Computer-Aided Engineering*, Vol. 9, No. 1, (Jan. 1999) (32-41), ISBN: 1096-4290.

Marzall, L. F., Schildberg, R. & Lacava, J. C. S. (2009), High-performance, low-cross-polarization suspended patch array for WLAN applications, *Proceedings of Antennas and Propagation Society International Symposium*, pp. 1-4, ISBN: 978-1-4244-3647-7, Charleston, SC, USA, June 2009.

Marzall, L. F., Nascimento D.C., Schildberg, R. & Lacava, J. C. S. (2010), An effective strategy for designing probe-fed linearly-polarized thick microstrip arrays with symmetrical return loss bandwidth, *PIERS Online*, Vol. 6, No. 8, (July 2010) (700-704), ISSN: 1931-7360.

Nascimento, D. C.; Mores Jr., J.A.; Schildberg, R. & Lacava, J. C. S. (2006), Low-cost truncated corner microstrip antenna for GPS application, *Proceedings of Antennas and Propagation Society International Symposium*, pp. 1557-1560, ISBN: 1-4244-0123-2, Albuquerque, NM, USA, July 2006.

Nascimento, D. C.; Bianchi, I.; Schildberg, R. & Lacava, J. C. S. (2007a), Design of probe-fed truncated corner microstrip antennas for Globalstar system, *Proceedings of Antennas and Propagation Society International Symposium*, pp. 3041-3044, ISBN: 978-1-4244-0877-1, Honolulu, HI, USA, June 2007.

Nascimento, D. C.; Schildberg, R. & Lacava, J. C. S. (2007b), New considerations in the design of low-cost probe-fed truncated corner microstrip antennas for GPS applications, *Proceedings of Antennas and Propagation Society International Symposium*, pp. 749-752, ISBN: 978-1-4244-0877-1, Honolulu, HI, USA, June 2007.

Nascimento, D. C.; Schildberg, R. & Lacava, J. C. S. (2008). Design of low-cost microstrip antennas for Glonass applications. *PIERS Online*, Vol. 4, No. 7, (2008) (767-770), ISSN: 1931-7360.

Nascimento, D. C. & Lacava, J. C. S. (2009), Circularly-polarized microstrip antenna radiation efficiency simulation based on the Wheeler cap method, *Proceedings of Antennas and Propagation Society International Symposium*, pp. 1-4, ISBN: 978-1-4244-3647-7, Charleston, SC, USA, June 2009.

Niroojazi, M. & Azarmanesh, M. N. (2004), Practical design of single feed truncated corner microstrip antenna, *Proceedings of Second Annual Conference on Communication Networks and Services Research, 2004*, pp. 25-29, ISBN: 0-7695-2096-0, Fredericton, NB, Canada, May 2004.

Pozar, D. M. & Kaufman, B. (1988), Comparison of three methods for the measurement of printed antennas efficiency, *IEEE Transactions on Antennas and Propagation*, Vol. 36, No. 1, (Jan. 1988) (136-139), ISSN: 0018-926X.

Richards, W. F.; Lo, Y. T. & Harrison, D. D. (1981), An improved theory for microstrip antennas and applications, *IEEE Transactions on Antennas and Propagation*, Vol. 29, No 1, (Jan. 1981) (38-46), ISSN: 0018-926X.

Sona, K. S. & Rahmat-Samii, Y. (2006), On the implementation of Wheeler cap method in FDTD, *Proceedings of Antennas and Propagation Society International Symposium*, pp. 1445-1448, ISBN: 1-4244-0123-2, Albuquerque, NM, USA, July 2006.

Teng, P. L.; Tang, C. L. & Wong, K. L. (2001), A broadband planar patch antenna fed by a short probe feed, *Proceedings of Asia-Pacific Microwave Conference*, pp. 1243-1246, ISBN: 0-7803-7138-0, Taipei, China, Dec. 2001.

Tinoco S., A. F.; Nascimento, D. C. & Lacava, J. C. S. (2008), Rectangular microstrip antenna design suitable for undergraduate courses, *Proceedings of Antennas and Propagation Society International Symposium*, pp. 1-4, ISBN: 978-1-4244-2041-4, San Diego, CA, USA, July 2008.

Tzeng, Y. B.; Su, C. W. & Lee, C. H. (2005), Study of broadband CP patch antenna with its ground plane having an elevated portion, *Proceedings of Asia-Pacific Microwave Conference*, pp. 1-4, ISBN: 0-7803-9433-X, Suzhou, China, Dec. 2005

Vandenbosch, G. A. E. & Van de Capelle, A. R. (1994), Study of the capacitively fed microstrip antenna element, *IEEE Transactions on Antennas and Propagation*, Vol. 42, No. 12, (Dec. 1994) (1648-1652), ISSN: 0018-926X.

Volakis, J. L. (2007). *Antenna Engineering Handbook. 4th ed.*, McGraw-Hill, ISBN: 0-07-147574-5, New York.

Wheeler, H. A. (1959), The radiansphere around a small antenna, *Proceedings of the IRE*, Vol. 47, No. 8, (Aug. 1959) (1325-1331), ISSN: 0096-8390.

Microstrip Antennas

Edited by Prof. Nasimuddin Nasimuddin

ISBN 978-953-307-247-0
Hard cover, 540 pages
Publisher InTech
Published online 04, April, 2011
Published in print edition April, 2011

In the last 40 years, the microstrip antenna has been developed for many communication systems such as radars, sensors, wireless, satellite, broadcasting, ultra-wideband, radio frequency identifications (RFIDs), reader devices etc. The progress in modern wireless communication systems has dramatically increased the demand for microstrip antennas. In this book some recent advances in microstrip antennas are presented.

InTech Europe
University Campus STeP Ri
Slavka Krautzeka 83/A
51000 Rijeka, Croatia
Phone: +385 (51) 770 447
Fax: +385 (51) 686 166
www.intechopen.com

InTech China
Unit 405, Office Block, Hotel Equatorial Shanghai
No.65, Yan An Road (West), Shanghai, 200040, China
中国上海市延安西路65号上海国际贵都大饭店办公楼405单元
Phone: +86-21-62489820
Fax: +86-21-62489821

IntechOpen